



HAL
open science

Modelization of boundary friction damping induced by second-order bending strain

Yifan Yang, Louis Jézéquel, Olivier Dessombz, Philippe Bristiel, Olivier Sauvage

► **To cite this version:**

Yifan Yang, Louis Jézéquel, Olivier Dessombz, Philippe Bristiel, Olivier Sauvage. Modelization of boundary friction damping induced by second-order bending strain. *Journal of Sound and Vibration*, 2019, 446, pp.113 - 128. 10.1016/j.jsv.2019.01.033 . hal-03486023

HAL Id: hal-03486023

<https://hal.science/hal-03486023v1>

Submitted on 20 Dec 2021

HAL is a multi-disciplinary open access archive for the deposit and dissemination of scientific research documents, whether they are published or not. The documents may come from teaching and research institutions in France or abroad, or from public or private research centers.

L'archive ouverte pluridisciplinaire **HAL**, est destinée au dépôt et à la diffusion de documents scientifiques de niveau recherche, publiés ou non, émanant des établissements d'enseignement et de recherche français ou étrangers, des laboratoires publics ou privés.



Distributed under a Creative Commons Attribution - NonCommercial 4.0 International License

Modelization of Boundary Friction Damping Induced by Second-Order Bending Strain

Yifan YANG^{a,*}, Louis JEZEQUEL^a, Olivier DESSOMBZ^a, Philippe BRISTIEL^b, Olivier SAUVAGE^c

^a*Ecole Centrale de Lyon, Laboratoire de Tribologie et Dynamique des Systèmes
36 avenue Guy de Collongue, 69130 Ecully, France*

^b*Groupe PSA*

2-10 boulevard de l'Europe, 78300 Poissy, France

^c*Groupe PSA, Scientific and Future Technologies Department / StelLab
route de Gisy, 78140 Vélizy-Villacoublay, France*

Abstract

Damping induced by frictional slipping in assembled structures is always a difficulty in vibration mechanics. Sometimes the cycling movement in riveted or bolted joint is generated by in-plane force field which is directly related to transverse deflection. Since this phenomenon cannot be described by classical plate theory, a general formulation based on von-Kármán plate theory is proposed in this study. The response estimation involving damping is conducted with the Krylov-Bogoliubov linearization method(HBM). The notion of non-linear mode is introduced in the context of single mode method and multi-mode method. The influence of mode shape change on forced response is also analyzed.

Keywords: damping, friction, von-Kármán plate, non-linear mode, linearization

1. Introduction

The prediction of fatigue endurance is a critical phase in engineering design, however a reliable assessment of fatigue property cannot be made without the knowledge of vibration amplitude. An accurate damping value is thus necessary but its estimation is always a challenging subject of research, especially in assembled mechanical systems. Damping takes mainly two energy dissipation forms: material damping and friction damping. The effect of material damping is present throughout the entire structure and influences all modes, it's generally considered as frequency-dependent. But friction damping resulting from bolted or riveted joints occurs locally and appears amplitude-dependent. Friction damping is normally about 10-100 times higher than material damping, therefore it plays a dominant role in determining the vibratory response of the structure [1]. The key to reliable response estimation is thus in the accurate modelization of friction damping.

*Corresponding author. Tel.: (+33) 6 70 01 98 82.
Email address: yangyifan5558@gmail.com (Yifan YANG)

A general overview of various friction damping models was given by Gaul [2]. The work of Bograd shows that joint damping in tangential direction significantly exceeds damping in normal direction [3]. The study of energy dissipation due to tangential relative displacement was firstly introduced by analytical approach on a simplified lap joint [4]. Sandwich beam model was then exploited by Masuko and Nishiwaki [5, 6], in which the displacement dependence of frictional damping was verified and the existence of optimum interface pressure was confirmed. Nanda and Singh extended the analytical two-layered sandwich beam to multi-layered structures [7, 8] and found that an increase in number of layers could improve substantially the damping capacity of jointed structures. The influence of non-uniform pressure at contact interface was analyzed by Damisa and he discovered the possibility of an optimized energy dissipation under non-uniform clamping pressure profile [9, 10]. There exists other analytical friction models such as one-dimensional micro-slip friction model [11], clamped circular plate model [12] and clamped-clamped zero-bending model [13], these models are all one-dimensional and are developed from a static point of view which prohibits them from taking into account the dynamic coupling between modes.

Apart from laminated beams, there are also a large number of structures in the form of plate whose tangential displacement in the joint is induced by transverse deflection. The in-plane force field due to second order strain results in a cycling shrink movement at the slipping interface, which forms a mechanism of energy dissipation. This phenomenon was firstly studied by [14] on hinged bars, which was still in the realm of one-dimensional analysis. The equilibrium with second-order strain in two dimensions can be described by von-Kármán plate theory. The dynamic solution of von-Kármán equations was proposed in [15, 16], but contact property was not involved in the development. The solution existence of von-Kármán plate involving contact was given by [17], however the influence of friction was not mentioned in this research.

The aim of the current study is to model damping induced by boundary slipping in von-Kármán plate, which is a phenomenon frequently observed in bolted or riveted structures. In the first part, the application of fictive force field is justified from the equilibrium equation with non-linear second-order strain. This method enables a model dimension reduction and diminishes the time of calculation. The second part demonstrates the solution procedure for von-Kármán equations in the case of forced vibration. It is based on Rayleigh-Ritz method and Krylov-Bogoliubov(HBM) linearization. The third part deals with a coupled system that can be solved by either single mode method or multi-mode method. The response of the whole system can be synthesized to hardening and damping factors who are in function of modal amplitude. The influence of boundary force conditions and mode shape changes are then analyzed.

2. Fictive force field

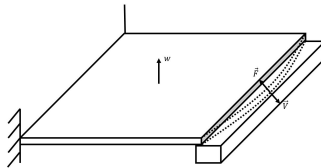


Figure 1: von-Kármán plate with frictional boundary

Nomenclature

(\mathbf{F}_{cr})	condensed reference fictive force vector	ρ	mass density per unit area
(\mathbf{F})	fictive force vector	σ_{ij}	stress components
$(\mathbf{N}_{\mathbf{B}})$	friction force vector	τ_x	tangential shear force in x direction
(\mathbf{U})	displacement vector	τ_y	tangential shear force in y direction
$[\mathbf{J}]$	Jacobian matrix	$\tilde{\omega}_k$	non-linear angular natural frequency of mode k
$[\mathbf{K}_{\text{c}}]$	condensed stiffness matrix	$\tilde{\phi}_k$	non-linear normalized mode shape of mode k
$[\mathbf{K}]$	plane stress stiffness matrix	\tilde{f}	non-linear modal force
$[\mathbf{R}]$	iso-parametric element shape function	\tilde{M}	non-linear modal mass
$[\Omega^2]$	diagonal spectral matrix	b_{kj}	mode participation factor
ΔW	energy dissipation per cycle	D	flectural rigidity
δ_{ij}	Kronecker δ	du	infinitesimal displacement increment in x direction
ϵ_{ij}	strain components	dv	infinitesimal displacement increment in y direction
η	damping factor	e	error function
\hat{q}	complex mode coordinate	E_{max}	maximum elastic energy in one cycle
λ	hardening factor	f_x	fictive force in x direction
\mathbf{B}	boundary DOFs	f_y	fictive force in y direction
\mathbf{I}	internal DOFs	N	in-plane force per unit length
μ	coefficient of friction	q	external excitation
∇	Laplacian operator	S^m	area of element m
ν	Poisson's ratio	t	step in quasi-static calculation
ω_k	angular natural frequency of mode k	u_{ij}	displacement components
ω_n	natural frequency in single mode method	w	transverse deflection
ϕ	normalized mode shape		
ϕ_k	normalized mode shape of mode k		

Similar to classical Kirchoff plate theory, von-Kármán's plate theory adopts the hypothesis that lines normal to the undeformed middle surface remain normal to this surface after deformation. The difference resides in the assumption that transversal equilibrium is not only guaranteed by bending rigidity D , but also balanced by in-plane forces for cases where their transversal direction projections cannot be neglected. As figure 1 illustrates, the slipping end shrinks under an imposed form on the plate. This theory enables a coupling between in-plane forces N_x , N_y and N_{xy} and

transversal displacement $w(x, y, t)$ of the plate. The local dynamic equilibrium equation is written as

$$\rho \frac{\partial^2 w}{\partial t^2} + D \Delta^4 w - \left(N_x \frac{\partial^2 w}{\partial x^2} + 2N_{xy} \frac{\partial^2 w}{\partial x \partial y} + N_y \frac{\partial^2 w}{\partial y^2} \right) = q(x, y, t) \quad (1)$$

with

$$N_x = \int_0^h \sigma_x dz, \quad N_{xy} = \int_0^h \sigma_{xy} dz, \quad N_y = \int_0^h \sigma_y dz \quad (2)$$

where ρ is density, h is thickness of the plate, Δ^2 is Laplacian operator, D is bending rigidity of the plate given by $D = Eh^3/12(1 - \nu^2)$ and $q(x, y, t)$ is exterior loading at a given position (x, y) and given time t .

The components of the three-dimensional Lagrangian Green strain tensor are defined as

$$E_{ij} = \frac{1}{2} \left(\frac{\partial u_i}{\partial x_j} + \frac{\partial u_j}{\partial x_i} + \frac{\partial u_k}{\partial x_i} \frac{\partial u_k}{\partial x_j} \right), \quad k = 1, 2, 3. \quad (3)$$

The von-Kármán plate theory takes into account the non-linear second-order strain components that are contributed by transverse deflection, the contributions from the in-plane directions x and y are neglected and the index k is only valued at 3. The strains can thus be expressed as

$$\epsilon_x = \frac{\partial u}{\partial x} + z \frac{\partial^2 w}{\partial x^2} + \frac{1}{2} \left(\frac{\partial w}{\partial x} \right)^2 \quad (4a)$$

$$\epsilon_y = \frac{\partial v}{\partial y} + z \frac{\partial^2 w}{\partial y^2} + \frac{1}{2} \left(\frac{\partial w}{\partial y} \right)^2 \quad (4b)$$

$$\epsilon_{xy} = \frac{1}{2} \left(\frac{\partial u}{\partial y} + \frac{\partial v}{\partial x} + z \frac{\partial^2 w}{\partial x \partial y} + \frac{\partial w}{\partial x} \frac{\partial w}{\partial y} \right). \quad (4c)$$

By using Hooke's law which establishes the relationship between stresses and strains

$$\sigma_{ij} = \frac{E}{1 - \nu^2} [(1 - \nu)\epsilon_{ij} + \nu\epsilon_{kk}\delta_{ij}], \quad \delta_{ij} : \text{Kronecker } \delta \quad (5)$$

and integrating along the thickness of the plate based on equation 2, the averaged in-plane stresses can be calculated by N_{ij}/h and expressed by

$$\sigma_x = \frac{E}{1 - \nu^2} \left\{ \left[\frac{\partial u}{\partial x} + \frac{1}{2} \left(\frac{\partial w}{\partial x} \right)^2 \right] + \nu \left[\frac{\partial v}{\partial y} + \frac{1}{2} \left(\frac{\partial w}{\partial y} \right)^2 \right] \right\} \quad (6a)$$

$$\sigma_y = \frac{E}{1 - \nu^2} \left\{ \left[\frac{\partial v}{\partial y} + \frac{1}{2} \left(\frac{\partial w}{\partial y} \right)^2 \right] + \nu \left[\frac{\partial u}{\partial x} + \frac{1}{2} \left(\frac{\partial w}{\partial x} \right)^2 \right] \right\} \quad (6b)$$

$$\sigma_{xy} = \frac{E}{2(1 + \nu)} \left(\frac{\partial u}{\partial y} + \frac{\partial v}{\partial x} + \frac{\partial w}{\partial x} \frac{\partial w}{\partial y} \right). \quad (6c)$$

The components of the in-plane stresses can be divided into two parts: one part is a function of in-plane displacements u and v and another part is a function of transverse displacement w .

Substituting the stress components into the infinitesimal equilibrium equation

$$\sigma_{ij,j} + f_i = 0, \quad (7)$$

the local equilibrium equation in terms of displacements u , v and w can be obtained. Take the equilibrium in x direction as example

$$\begin{aligned} \frac{E}{1-\nu^2} \frac{\partial}{\partial x} \left\{ \left[\frac{\partial u}{\partial x} + \frac{1}{2} \left(\frac{\partial w}{\partial x} \right)^2 \right] + \nu \left[\frac{\partial v}{\partial y} + \frac{1}{2} \left(\frac{\partial w}{\partial y} \right)^2 \right] \right\} \\ + \frac{E}{2(1+\nu)} \frac{\partial}{\partial y} \left(\frac{\partial u}{\partial y} + \frac{\partial v}{\partial x} + \frac{\partial w}{\partial x} \frac{\partial w}{\partial y} \right) = 0 \end{aligned} \quad (8)$$

and separate the components induced by transverse deflection from the those related to in-plane displacements

$$\begin{aligned} \frac{E}{1-\nu^2} \frac{\partial}{\partial x} \left(\frac{\partial u}{\partial x} + \nu \frac{\partial v}{\partial y} \right) + \frac{E}{2(1+\nu)} \frac{\partial}{\partial y} \left(\frac{\partial u}{\partial y} + \frac{\partial v}{\partial x} \right) \\ + \frac{E}{1-\nu^2} \frac{\partial}{\partial x} \left[\frac{1}{2} \left(\frac{\partial w}{\partial x} \right)^2 + \frac{\nu}{2} \left(\frac{\partial w}{\partial y} \right)^2 \right] + \frac{E}{2(1+\nu)} \frac{\partial}{\partial y} \left(\frac{\partial w}{\partial x} \frac{\partial w}{\partial y} \right) = 0. \end{aligned} \quad (9)$$

Since the body force f_i doesn't exist, the current problem can be regarded as being transformed into a plane stress equilibrium problem with first order linear strain, the excitation comes from a fictive body force field which is induced by transverse deflection. The fictive body force in the x and y direction can thus be written as

$$f_x = \frac{E}{1-\nu^2} \left(\frac{\partial w}{\partial x} \frac{\partial^2 w}{\partial x^2} + \nu \frac{\partial w}{\partial y} \frac{\partial^2 w}{\partial x \partial y} \right) + \frac{E}{2(1+\nu)} \left(\frac{\partial^2 w}{\partial x \partial y} \frac{\partial w}{\partial y} + \frac{\partial w}{\partial x} \frac{\partial^2 w}{\partial y^2} \right) \quad (10a)$$

$$f_y = \frac{E}{1-\nu^2} \left(\frac{\partial w}{\partial y} \frac{\partial^2 w}{\partial y^2} + \nu \frac{\partial w}{\partial x} \frac{\partial^2 w}{\partial x \partial y} \right) + \frac{E}{2(1+\nu)} \left(\frac{\partial^2 w}{\partial x \partial y} \frac{\partial w}{\partial x} + \frac{\partial w}{\partial y} \frac{\partial^2 w}{\partial x^2} \right). \quad (10b)$$

The fictive body force field is a function of transverse displacement's spatial first and second derivatives and they can be calculated by finite difference method. This fictive field enables the solution of in-plane displacements u and v with a given w which originates from a known mode shape. Once u and v are known, they can be substituted in equation 6 to yield the superimposed in-plane stress field.

3. Friction properties

The contact property used in the current study is a two-dimensional Coulomb's friction law. The shear stress components on the contact surface are designated as τ_x and τ_y and normal stress as

σ_n . When the boundary is in sticking phase, the static frictional force is in the direction of reaction force. However once the shear stress resultant is bigger than the maximum frictional stress limit, the slipping occurs and the direction of frictional force is in the direction of relative displacement speed.

In case of sticking, the shear resultant is inferior to the maximum shear stress

$$(\tau_x^2 + \tau_y^2)^{\frac{1}{2}} < \mu\sigma_n. \quad (11)$$

In case of slipping, the stress resultant is saturated to the value of maximum shear stress $\mu\sigma_n$ and the friction's direction can be determined by the speed direction of the relative displacement. The speed can be replaced by infinitesimal displacement increment du/dt and dv/dt . As the frictional force is always in the opposite direction of speed, a negative sign is added to the component du and dv .

$$(\tau_x^2 + \tau_y^2)^{\frac{1}{2}} = \mu\sigma_n \quad (12a)$$

$$\tau_x = \mu\sigma_n \cdot \frac{-du}{\sqrt{du^2 + dv^2}} \quad (12b)$$

$$\tau_y = \mu\sigma_n \cdot \frac{-dv}{\sqrt{du^2 + dv^2}}. \quad (12c)$$

The frictional property at the contact interface can be combined to the fictive force field to establish the in-plane equilibrium, from which the slipping displacement can be cumulated to calculate the total energy dissipation during one cycle in periodic movement. The next section will present the solution procedure which is based on Ritz-Galerkin method.

4. Solution procedure

The in-plane problem can be solved by finite element method. Plane stress elements are used for discretization. By using the shape function of iso-parametric 4-node element, the equivalent nodal forces of a given element m can be expressed as

$$(\mathbf{f}_m) = \int_{-1}^1 \int_{-1}^1 [\mathbf{R}]^T \begin{pmatrix} f_x \\ f_y \end{pmatrix} h |\mathbf{J}| ds dt. \quad (13)$$

Where $[\mathbf{R}]$ is a (8×2) matrix of shape functions, $|\mathbf{J}|$ is the determinant of Jacobian matrix and h is the thickness of the plate. The global equilibrium equation can be written as

$$\begin{bmatrix} \mathbf{K}_{II} & \mathbf{K}_{IB} \\ \mathbf{K}_{BI} & \mathbf{K}_{BB} \end{bmatrix} \begin{pmatrix} \mathbf{U}_I \\ \mathbf{U}_B \end{pmatrix} = \begin{pmatrix} \mathbf{F}_I \\ \mathbf{F}_B \end{pmatrix} + \begin{pmatrix} \mathbf{0} \\ \mathbf{N}_B \end{pmatrix} \quad (14)$$

where index I and B corresponds respectively to inner and boundary DOFs. The vector \mathbf{F} , assembled from the equivalent nodal forces (\mathbf{f}_m) of each element, contains the discretized fictive body force field. The vector \mathbf{N} is the frictional force at the boundary which respects the friction law presented in the previous section. Since there is no frictional force on inner DOFs, the corresponding components in \mathbf{N} are $\mathbf{0}$. Since there is no friction forces on inner DOFs, the model can be

condensed to boundary DOFs and thus result in a smaller model with less DOFs. The condensed form is

$$[\mathbf{K}_c](\mathbf{U}_B) = (\mathbf{F}_c) + (\mathbf{N}_B) \quad (15)$$

where the condensed stiffness matrix $[\mathbf{K}_c]$ and fictive force vector (\mathbf{F}_c) are respectively written as

$$[\mathbf{K}_c] = [\mathbf{K}_{BB}] - [\mathbf{K}_{BI}][\mathbf{K}_{II}]^{-1}[\mathbf{K}_{IB}] \quad (16a)$$

$$(\mathbf{F}_c) = (\mathbf{F}_B) - [\mathbf{K}_{BI}][\mathbf{K}_{II}]^{-1}(\mathbf{F}_I). \quad (16b)$$

In order to control the amplitude of transverse deflection, which is to be transformed into fictive force field by equation 10, the mode shape normalized to mass matrix is written as ϕ in the following sections. The real amplitude w can thus be expressed as

$$w = q\phi. \quad (17)$$

At the initialization step of the calculation, all boundary DOFs who have potential to slip are blocked. The trial reaction friction forces (\mathbf{N}_B) of step $t + 1$ are evaluated from the previous step's displacement

$$(\mathbf{N}_B)_{t+1} = [\mathbf{K}_c](\mathbf{U}_B)_t - q_{t+1}^2(\mathbf{F}_{cr}) \quad (18)$$

where (\mathbf{F}_{cr}) is the condensed reference body force field obtained from the normalized mode shape ϕ .

The obtained $(\mathbf{N}_B)_{t+1}$ should satisfy the sticking-slipping criteria in equation 11 and 12. The updated friction force $(\mathbf{N}_B)_{t+1}^{new}$ can then be carried into the equilibrium of step $t + 1$ to calculate the real boundary displacement

$$(\mathbf{U}_B)_{t+1} = [\mathbf{K}_c]^{-1} (q_{t+1}^2(\mathbf{F}_{cr}) + (\mathbf{N}_B)_{t+1}^{new}). \quad (19)$$

The displacement of other DOFs at each step t can be obtained by reversing the condensation procedure with the known boundary displacement

$$(\mathbf{U}_I)_t = [\mathbf{K}_{II}]^{-1} (q_t^2(\mathbf{F}_I)_t - [\mathbf{K}_{IB}](\mathbf{U}_B)_t). \quad (20)$$

Since u and v are all known, the superimposed in-plane stress field can thus be obtained with equation 6 and the solution of equation 1 is possible. By applying the notion of modal synthesis, the transverse deflection of the plate can be approximated by a linear combination of n first normal modes ϕ_k . The normal modes are a solution of eigenvalue problem defined in linear plate theory

$$D\nabla^4\phi_k = \omega_k^2\rho\phi_k. \quad (21)$$

Since the linear combination of ϕ_k is only an approximation, the error expression of equation 1 can be written as

$$e = \sum_{k=1}^n \frac{d^2q_k}{dt^2} \rho\phi_k + \sum_{k=1}^n q_k D\nabla^4\phi_k - \sum_{k=1}^n q_k R(N, \phi_k) - q(x, y, t) \quad (22)$$

where the non-linear term is abbreviated as $R(N, \phi_k)$ where

$$R(N, \phi_k) = \sum_{k=1}^n \left(N_x \frac{\partial^2 \phi_k}{\partial x^2} + 2N_{xy} \frac{\partial^2 \phi_k}{\partial x \partial y} + N_y \frac{\partial^2 \phi_k}{\partial y^2} \right). \quad (23)$$

In the current study, we are only interested in mono-mode response of the structure excited in the neighborhood of its resonance frequency ω_k , therefore the mode shape ϕ_k is dominant in the response and we consider in the first place that the shape of mode k doesn't change with amplitude. Thus only the mode shape ϕ_k is retained in equation 22. The Ritz-Galerkin method can be used to minimize the error function e

$$\int_s \frac{d^2 q}{dt^2} \rho \phi_k \phi_k ds + \int_s q D \nabla^4 \phi_k \phi_k ds - \int_s q R(N, \phi_k) \phi_k ds = \int_s q(x, y, t) \phi_k ds. \quad (24)$$

Since the mode ϕ_k is normalized in the way

$$\int_s \rho \phi_k \phi_k ds = 1, \quad (25)$$

the error function can be written in scalar form as

$$\frac{d^2 q}{dt^2} + \omega_k^2 q - \psi(t)q = f(t) \quad (26)$$

where

$$\psi_{kk}(t) = \int_s R(N, \phi_k) \phi_k ds. \quad (27)$$

The N_{ix} , N_{iy} and N_{ixy} are valued at the center of each element m for mode i and are assumed to be homogeneous within the given element. The spatial first and second derivatives are obtained by finite difference method. The discretized expression of ψ_{ii} takes the form

$$\psi_{kk} = \sum_{m=1}^N \left(N_x^m \frac{\partial^2 \phi_k^m}{\partial x^2} + 2N_{xy}^m \frac{\partial^2 \phi_k^m}{\partial x \partial y} + N_y^m \frac{\partial^2 \phi_k^m}{\partial y^2} \right) \phi_k^m S^m \quad (28)$$

with S^m the surface area of element m , N the total number of elements.

The steady state solution for q under harmonic excitation of angular frequency ω is assumed in the form of a harmonic function of time. The excitation force's phase is taken as reference, and the phase angle is represented by a complex number \hat{q} .

$$q = \hat{q} e^{i\omega t}, \quad f = f e^{i\omega t} \quad (29)$$

Equation 26 becomes

$$-\omega^2 \hat{q} e^{i\omega t} + \omega_k^2 \hat{q} e^{i\omega t} - \psi(t) \hat{q} e^{i\omega t} = f e^{i\omega t}. \quad (30)$$

By equating the imaginary part of equation 30

$$-\omega^2 \hat{q} \sin \omega t + \omega_k^2 \hat{q} \sin \omega t - \psi(t) \hat{q} \sin \omega t = f \sin \omega t. \quad (31)$$

Since $\psi(t)$ is also a function of time t , the $\sin \omega t$ cannot be eliminated from equation 31 directly. The use of Harmonic Balance Method requires decomposition of the term $\psi(t) \sin \omega t$ into two harmonic components.

$$\psi(t) \sin \omega t = \psi_c \cos \omega t + \psi_s \sin \omega t \quad (32)$$

where

$$\theta = \omega t \quad (33a)$$

$$\psi_c = \frac{1}{2\pi} \int_0^{2\pi} -\psi(t) \sin 2\theta d\theta \quad (33b)$$

$$\psi_s = \frac{1}{2\pi} \int_0^{2\pi} -\psi(t)(1 - \cos 2\theta) d\theta \quad (33c)$$

In order to have the same harmonic base, the rotational vector \hat{q} with $\cos \omega t$ has to be multiplied by i in order to rotate 90 degrees to have the same harmonic base.

$$(-\omega^2 + \omega_k^2 + i\psi_c + \psi_s)\hat{q} \sin \omega t = f \sin \omega t \quad (34a)$$

$$[-\omega^2 + \omega_k^2(1 + \lambda + i\eta)]\hat{q} = f \quad (34b)$$

where

$$\eta = \frac{\psi_c}{\omega_k^2}, \quad \lambda = \frac{\psi_s}{\omega_k^2} \quad (35)$$

The structure's hardening is proportional to the coefficient λ and damping is represented by η . The structural damping factor can be determined with greater precision by using the ratio between energy dissipation per cycle and maximum stocked elastic energy [18]. In the following calculation, the damping factor is defined as

$$\eta = \frac{1}{2\pi} \frac{\Delta W}{E_{max}} \quad (36)$$

with

$$\Delta W = \sum_{t=2}^T |(\mathbf{U}_B^t - \mathbf{U}_B^{t-1})^T (\mathbf{N}_B^t)|, \quad E_{max} = \frac{1}{2} |\hat{q}|^2 \omega_k^2 \quad (37)$$

The solution of equation 34 can be achieved by applying an iterative Newton method with initial q as static displacement f/ω_k^2 . In order to give a clarified view of the proposed method, the general steps of the solution is presented below.

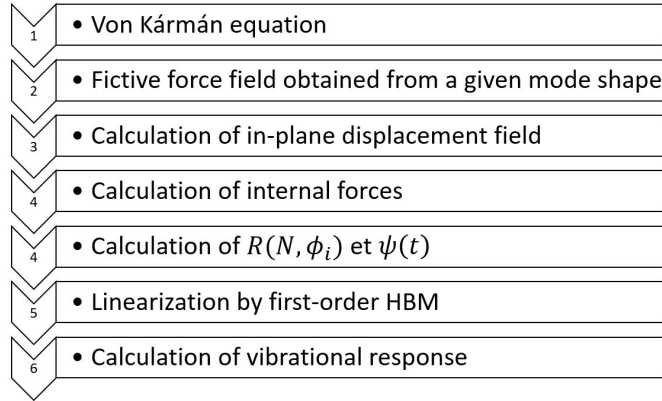


Figure 2: General steps of the solution method

5. Rectangular plate with two clamped edges

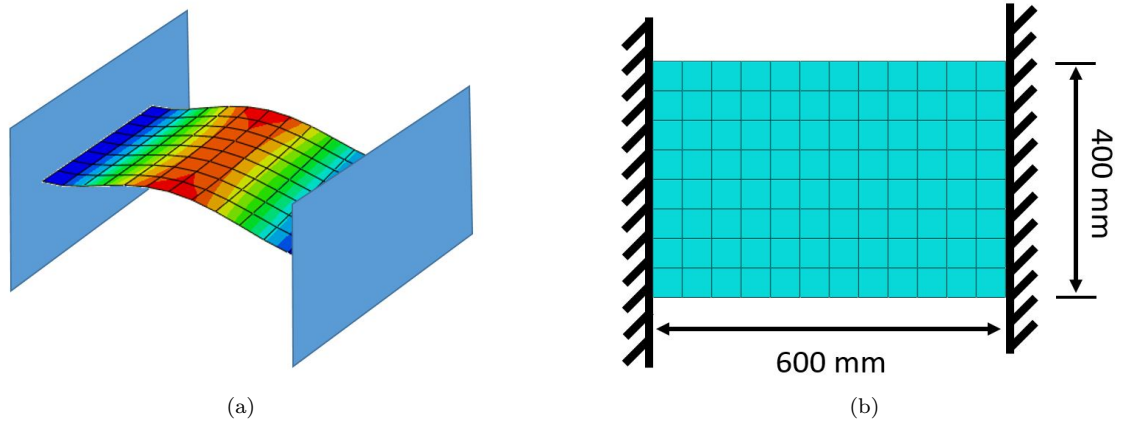


Figure 3: Only the first mode is retained

A rectangular plate of uniform thickness 2 mm is chosen to illustrate the hardening effect as well as the damping characteristics in von-Kármán plate. The length is 600 mm and the width is 400 mm. The plate is clamped at the boundary $x = 0$ and $x = 600$ mm and is excited by a cyclic force f at its first resonance frequency, which is 30.860 Hz. Since the first mode is dominant in the shape composition, according to the theory of single mode method, only the first linear mode is retained for the calculation of fictive force field. The clamped boundary condition can be assimilated to an infinite coefficient of friction.

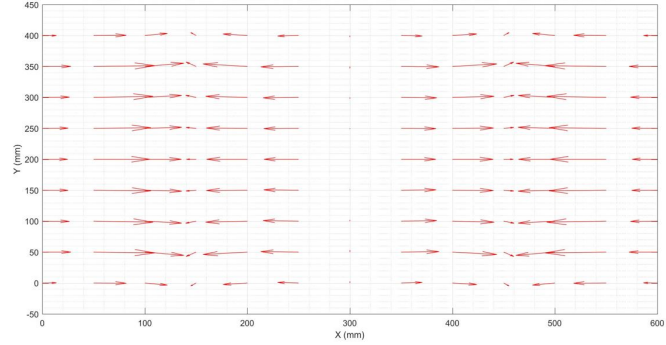


Figure 4: Fictive force field from the first mode

The in-plane fictive force field obtained from equation 10 is presented in figure 4. The DOFs on the middle line $x = 300$ mm is in equilibrium from the left and the right force field. However the DOFs on the line $x = 150$ mm and $x = 450$ mm are in compression. The non-zero derivatives in the y direction result in a field that is not exactly parallel to the x axis, especially for the points on the boundary $y = 0$ mm and $y = 400$ mm. The in-plane fictive force field engenders a non-uniform stress field in the plate, which generates a different ψ at each modal amplitude increment. After the temporal integral in equation 33, the hardening factor λ can be obtained. The damping factor is calculated from energy dissipation in equation 36. In the case of two clamped edges, the damping is not present due to the absence of dissipative mechanism.

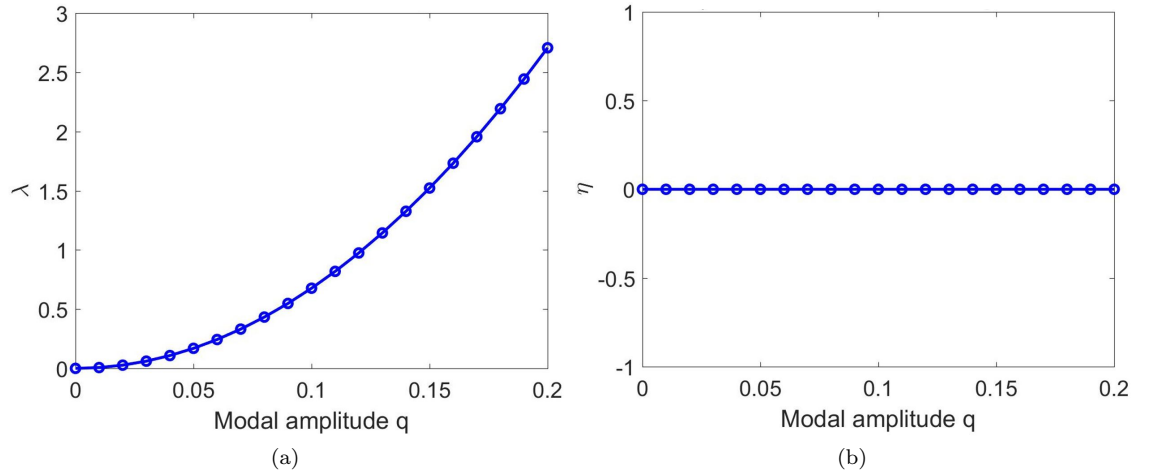


Figure 5: λ and η versus modal amplitude

The hardening factor increases with the increase in modal amplitude, which signifies that the structure becomes stiffer under bigger displacement.

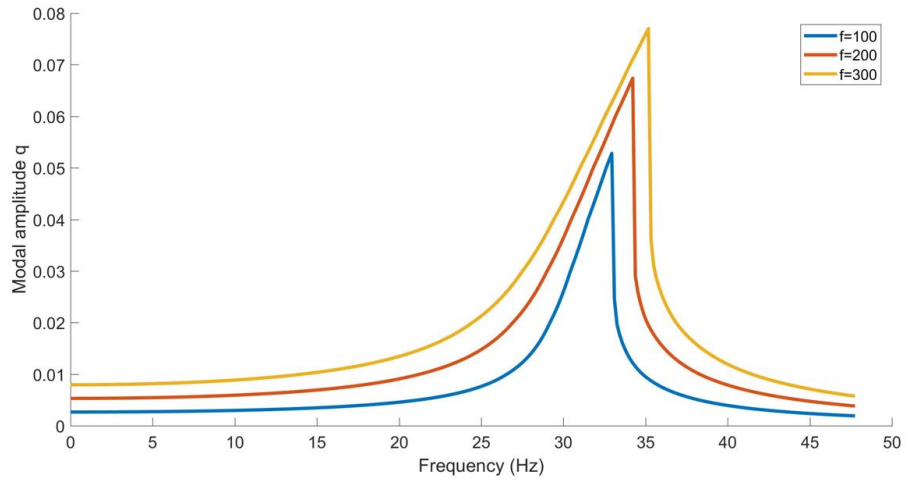


Figure 6: Frequency response curve under three different modal forces

The resonance moves towards higher frequencies due to the hardening effect. For any given frequency, bigger excitation forces result in larger displacement.

6. Rectangular plate with one slipping boundary

In the case with one slipping boundary, the left end is still clamped but the right end is subjected to a frictional clamp where the edge is supposed to slip for large modal amplitude. The contact area of 4000 mm^2 under the frictional clamp is considered to be constant, the coefficient of friction is fixed at 0.3.

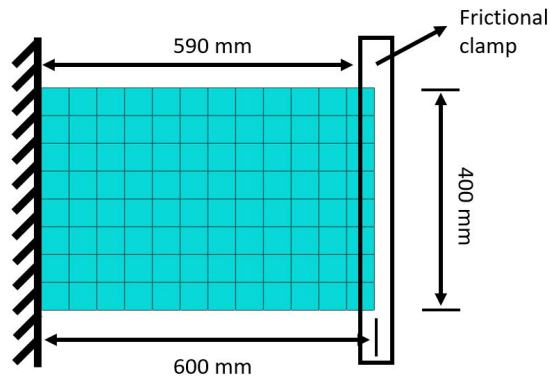


Figure 7: Rectangular plate with one slipping boundary

A fictive force field which corresponds to a maximum modal amplitude of 0.2 is applied to the in-plane problem, the frictional property used is presented in section 3, the clamping pressure is

0.5 MPa. The alternative sticking and slipping phases can be observed under two charging cycles. The frictional force increases during the sticking period and is saturated when the slipping occurs. The compression effect can also be observed from the fact that the right edge can no longer return to its original position, this phenomenon is produced in the relaxing phase by the frictional force which points to the clamped edge.

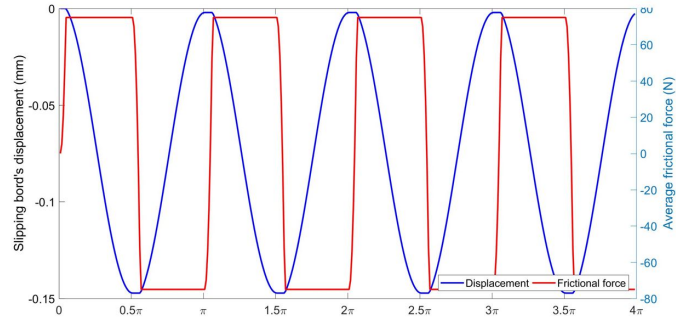


Figure 8: Average frictional force and displacement on the slipping edge

The hardening and damping factors are calculated under 3 different clamping pressures 0.5 MPa, 1 MPa and 2 MPa.

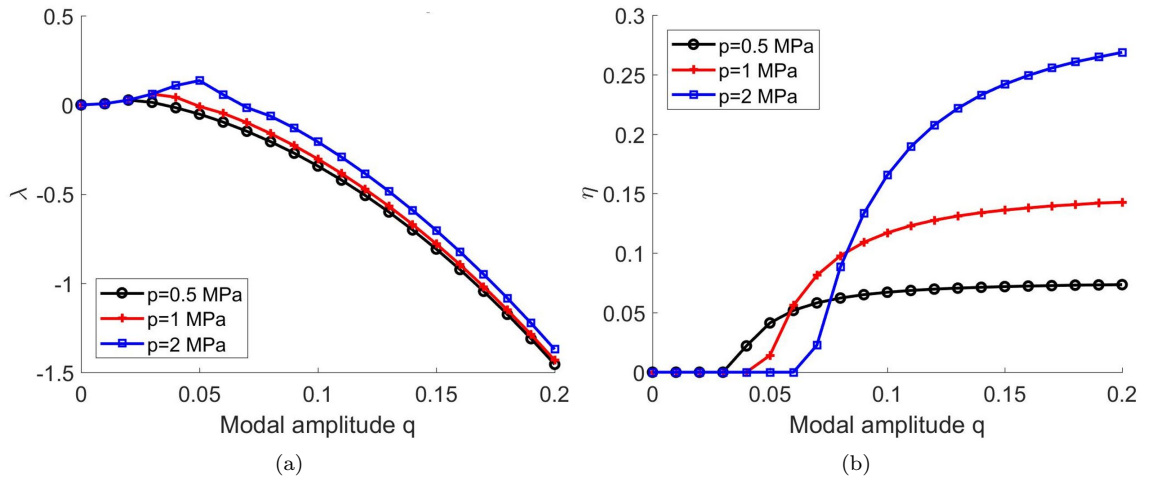


Figure 9: λ and η versus modal amplitude

When the modal amplitude is not big enough to activate boundary slipping, the $-\psi$ is always positive and the plate is under hardening effect. Once the modal amplitude is capable of activating slipping, the alternatively changing boundary condition will lead to a much more complicated stress field during one cycle and its overall influence is softening. By comparing the figure 9a and 9b, the softening effect is shown to appear earlier than the occurring of slipping. In the modal range which contains slipping, bigger modal amplitude will lead to a more softened structure.

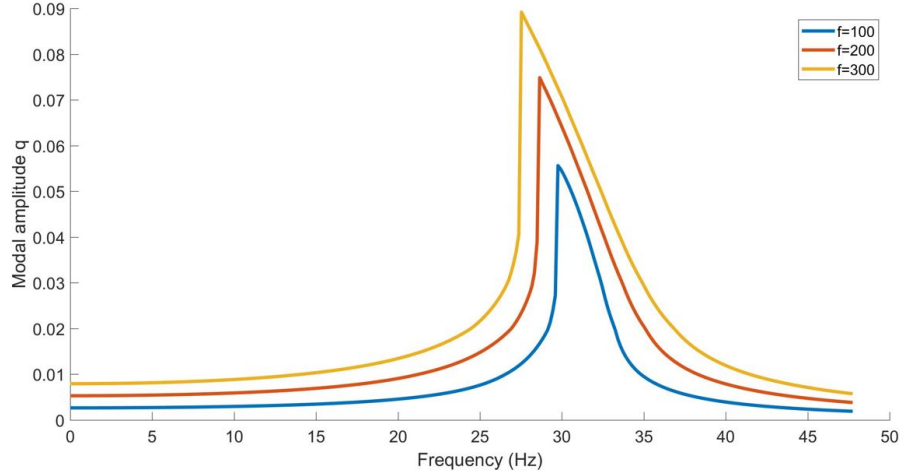


Figure 10: Frequency response curve with complete slipping boundary

The presence of slipping boundary changes the frequency-response property of the structure. In the range of the current excitation force, the structure becomes softer with a decreasing resonance frequency under bigger modal force, which corresponds to the monotone negative value range in figure 9a. The slipping boundary also results in a bigger modal response under the same excitation force compared to clamp-clamp boundary condition in figure 6. Compared to the effect of in-plane coupling, the influence of boundary slipping is shown to be more dominant in the response under big excitation force.

7. In the case of non-linear mode

The single mode method presented in the previous sections discounts the coupling between modes by non-linear terms. This coupling can be taken into account by using the notion of non-linear mode. The non-linear mode is defined by a linear superposition of linear modes

$$\tilde{\phi}_k = \sum_{j=1}^n b_{kj}(q)\phi_j \quad (38)$$

where ϕ_j is the j th linear mode and $b_{kj}(q)$ are participation factors of each mode with $b_{kk} = 1$, n is number of retained linear modes. This normalization is valid only in cases where the structure is excited at its k th natural frequency and it's the k th mode that is dominant in the shape composition. The participation factor is considered as a function of modal amplitude q and satisfies the initial condition $b_{kj}(q = 0) = 0$. The non-linear mode notion presented here is always in the realm of mono-mode response calculation, the only difference compared to single mode method is that the mode chosen retains no longer its shape, but changes in function of modal amplitude.

The values of b_{kj} are solutions of the following eigenfunction system which is derived from equation 24, 33 and 35.

$$-\tilde{\omega}_k^2(\mathbf{b}_{kj}) + ([\Omega^2] + [\lambda_{kj}])(\mathbf{b}_{kj}) = 0 \quad (39)$$

with

$$\lambda_{kj} = \frac{1}{2\pi} \int_0^{2\pi} (-\psi_{kj}(t))(1 - \cos 2\theta) d\theta. \quad (40)$$

The $\tilde{\omega}_k$ is the non-linear natural frequency corresponding to non-linear mode $\tilde{\phi}_k$, and it is also a function of modal amplitude q .

Similar to expression 28 in the single mode method, the discretized form of ψ_{kj} can be written as

$$\psi_{kj} = \sum_{m=1}^N \left(N_{jx}^m \frac{\partial^2 \phi_j^m}{\partial x^2} + 2N_{jxy}^m \frac{\partial^2 \phi_j^m}{\partial x \partial y} + N_{jy}^m \frac{\partial^2 \phi_j^m}{\partial y^2} \right) \phi_k^m S^m. \quad (41)$$

The coupling effect can be quantified by the participation factor b_{kj} , this non-linear mode approach is called multi-mode method in the following sections. The response of forced vibration in multi-mode method is given by complex amplitude \hat{q} , which is the solution of the following equation

$$[\tilde{M}(q)\omega^2 + \tilde{\omega}_k^2(q)(1 + i\eta(q))]\hat{q} = \tilde{f}(q) \quad (42)$$

where $\tilde{M}(q)$ is the non-linear modal mass and $\tilde{f}(q)$ is the non-linear modal force, $\eta(q)$ is calculated with the non-linear mode shape $\tilde{\phi}_k$.

$$\tilde{M}(q) = \sum_{j=1}^n b_{kj}^2(q), \quad \tilde{f}(q) = \sum_{j=1}^n b_{kj}(q)f_j \quad (43)$$

8. Multi-mode method with complete slipping boundary

In order to explain the notion of non-linear mode, a rectangular plate with one complete slipping boundary, as illustrated in figure 7, is used for explanation with three linear modes. Since the eigenvalue problem is a (3×3) system which has three eigenvalues, the one which is the closest to the linear resonance is retained as the non-linear resonance, the corresponding vector is the participation factors (\mathbf{b}_{kj}) .

In the first place, both the excitation and boundary conditions are considered symmetric, in this case anti-symmetric modes don't contribute to the response composition. The three linear modes retained here are all symmetric and are listed in figure below. The corresponding frequencies are respectively 30.86 Hz, 88.45 Hz and 98.19 Hz. The second and third mode are very close together.

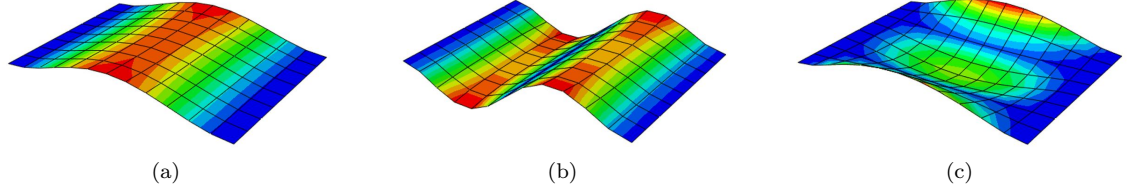


Figure 11: The three retained linear modes, mode 1 (a), mode 2 (b), mode 3 (c)

The coupling variable ψ_{kj} is valued at each time step in quasi-static calculation. The coupling effect in the frequency domain is directly related to the λ_{kj} obtained from temporal integral. After the normalization of the first mode participation factor to 1, the evolution of (\mathbf{b}_{ij}) in terms of modal amplitude q shows that b_{11} remains 1 while b_{12} and b_{13} stay 0 for all the amplitude range. This observation signifies that the second and third mode are not coupled with the first mode under symmetric boundary conditions. This phenomenon also justifies the application of single mode method.

In order to study the participation of anti-symmetric modes, it's necessary to break the symmetry by either applying an asymmetric pressure distribution or changing the kinematic boundary conditions. The influence of different clamping pressures is firstly presented in the following section.

9. Multi mode method with non-uniform clamping pressure

Based on the fact that the coupling coefficient ψ_{kj} is a function of internal stress field which is intrinsically sensitive to boundary pressures, it's necessary to clarify its influence on inter-mode coupling. Here a non-uniform clamping pressure is applied on the clamping pad. The pressure on the lower part is twice smaller than that on the upper part. Since the rotation of the boundary DOFs are always restrained by the clamp, the boundary conditions for both upper and lower nodes can be regarded as encastre. The parametric study in terms of modal amplitude shows that force boundary conditions have no significant influence on the evolution of participation factors. The second and third mode participation factors b_{12} and b_{13} stays 0 for all the amplitude range, which means that they are not coupled with the first mode and their participations can be neglected. It is thus reasonable to infer that the participation factor is only sensitive to linear mode shapes. This deduction is to be verified in the next section.

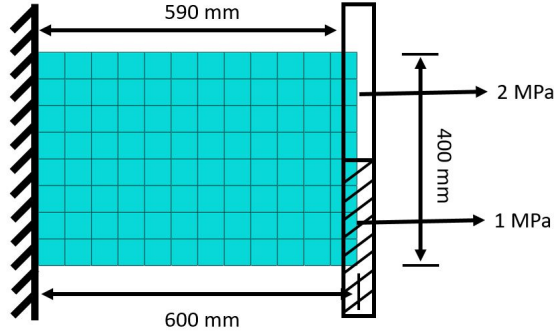


Figure 12: Rectangular plate with non-uniform clamping pressure

Even though the clamping pressures are not able to change the shape composition, the hardening and damping property are closely related to boundary forces. As the second and third mode are neglected, the fictive force field is generated only with the first mode shape. The comparison of coefficient λ and η under uniform and non-uniform clamping pressures are illustrated in figure below. The pressure is maintained at 2 MPa for the case with uniform clamping pressure.

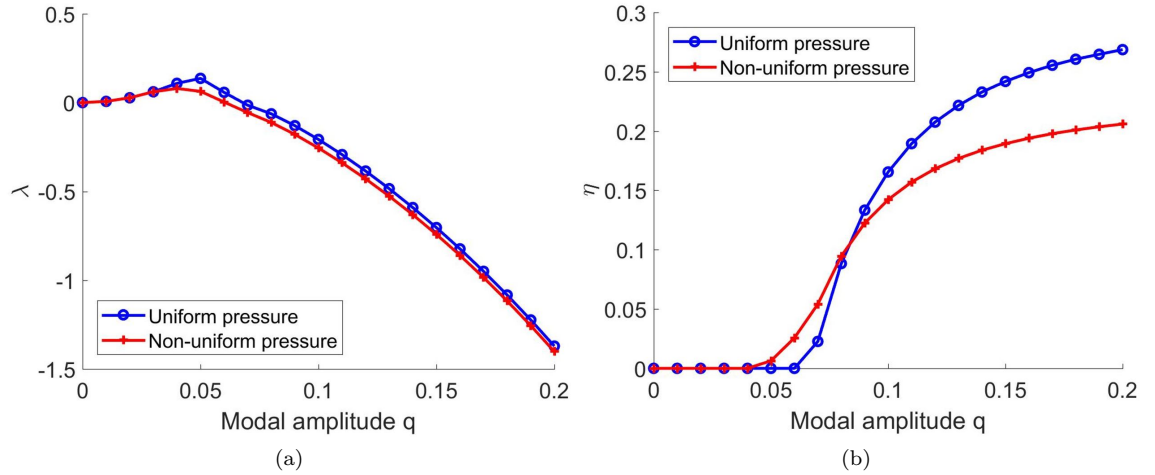


Figure 13: Influence of clamping pressure distribution of λ and η evolution

The structure is shown to be more solidified and damped with an uniform clamping pressure along the slipping boundary. The non-uniform clamp yields a smaller average pressure which enables earlier slipping, but the maximum damping capacity is weakened.

10. Multi mode method with half slipping boundary

A drastic way to break boundary condition symmetry is to completely remove the lower part of the clamping pad. This modification changes not only the force conditions, but also liberates the

lower part DOFs in the linear mode calculation. The clamping pressure in this example is fixed at 2 MPa.

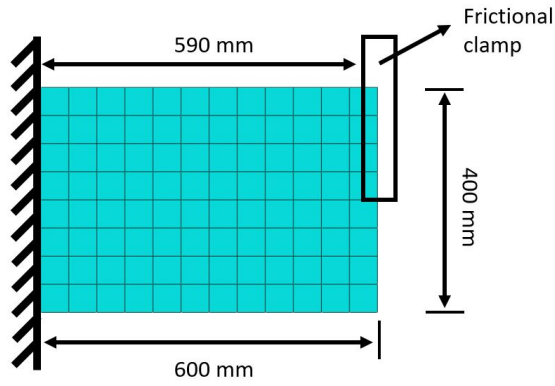


Figure 14: Rectangular plate with half slipping boundary

The first three modes retained for non-linear mode calculation as well as the corresponding fictive force fields are respectively illustrated in figure 15 and 16.

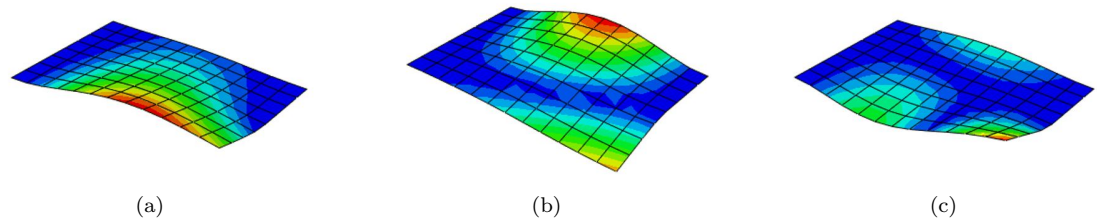


Figure 15: The three retained linear modes, mode 1 (a), mode 2 (b), mode 3 (c)

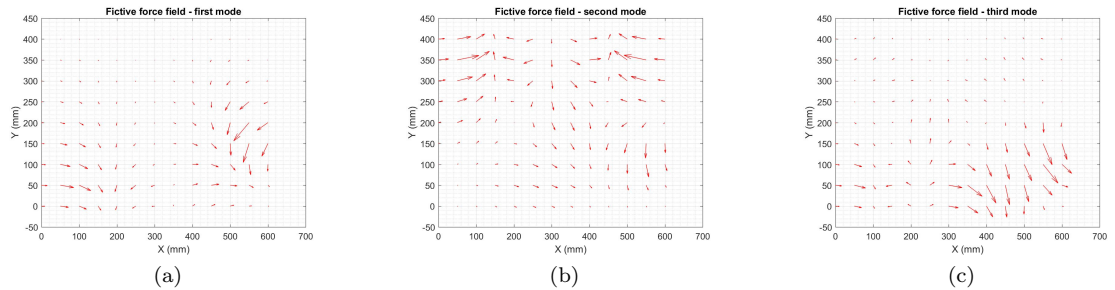


Figure 16: Fictive force fields of the three linear modes, mode 1 (a), mode 2 (b), mode 3 (c)

The non-symmetric mode shapes will result in non-symmetric force fields, which in consequence lead to stress fields that can be coupled together. The participation factor evolution in this case is presented in figure 17.

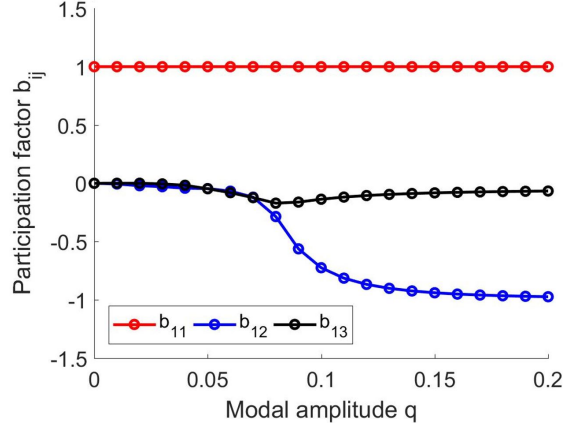


Figure 17: Participation factors with half slipping boundary

The second mode starts to participate in shape composition from modal amplitude of 0.05 and continues to be saturated at a constant level from 0.1. The participation of the third mode stays weak in all the range of modal amplitude. This result shows that for small modal amplitude, only one mode is sufficient to represent the overall vibration behavior of the structure, but for big modal amplitude, it's necessary to take into account the participation of other modes. In the current study, a modal amplitude of 0.05 corresponds to a physical displacement of 2 mm, which is the thickness of the plate, this deflection is already within the realm of large displacement and it is not likely to happen in vibration mechanics. Therefore the single mode method is sufficient for analysis with small displacement, even though the boundary conditions may yield inter-mode coupling, however for large modal amplitude, the participation of other modes cannot be neglected. The comparison of hardening factor λ and damping coefficient η obtained from single mode method and multi-mode method are illustrated in figure 18a and 18b.

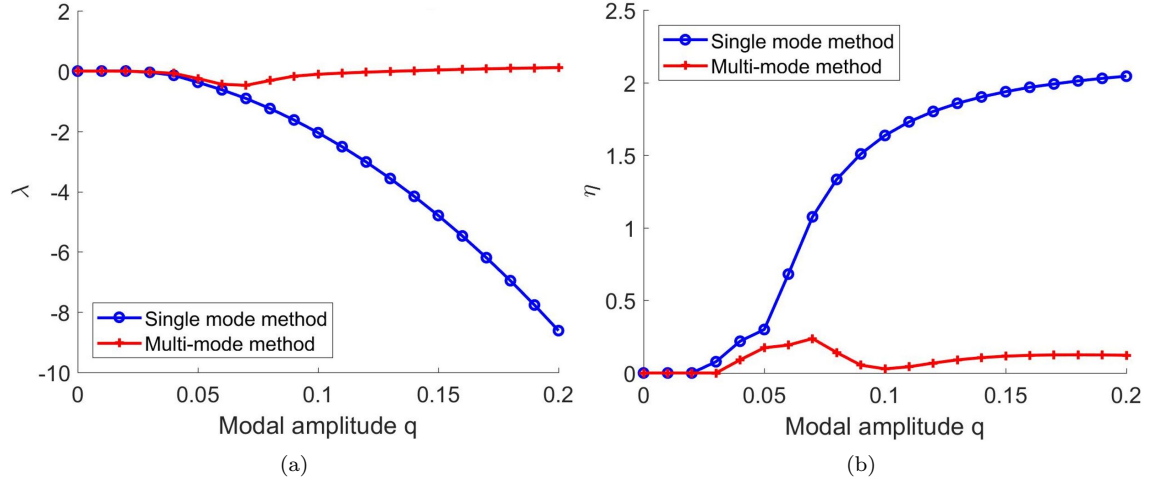


Figure 18: Influence of mode shape change on λ and η evolution

The comparison shows that hardening and damping are both sensitive to mode shape changes. The participation of second mode stops the on-going softening tendency and prohibits the damping capacity to grow. For small modal amplitude, it's acceptable to use only one mode shape to represent the vibration behavior since λ and η given by single and multi-mode method are almost the same, but for big modal amplitude, it's necessary to take into account the inter-mode coupling. An example of forced response is given with an oscillating excitation force applied at point A, as illustrated in figure 19. The excitation force amplitudes are respectively 10 N and 50 N for two different load cases.

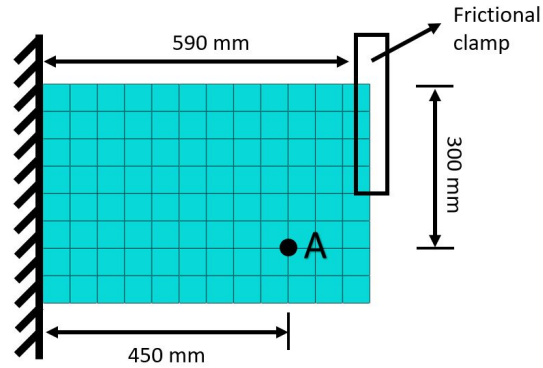


Figure 19: Excitation force position on the plate

The frequency-response curves in figure 20a and 20b demonstrate that for excitation forces who result in small modal amplitude, the coupling between modes is weak, so that single mode and multi-mode method provide very similar responses, however when the force is big enough to produce inter-mode coupling, the difference in response is no longer negligible. By comparing the response

amplitude at resonance, the single mode method always over-estimates the damping capacity compared to multi-mode method, but for frequencies outside the resonance zone, the amplitude is relatively small and the two methods give almost the same response level, which is in consistency with the λ and η curves.

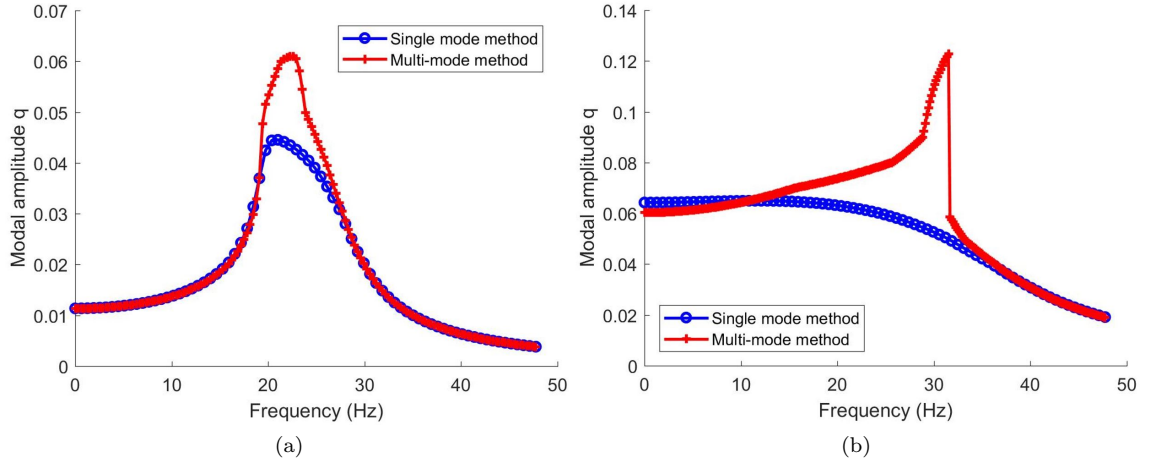


Figure 20: Influence of mode shape change on frequency response under $f = 10N$ (a) and $f = 50N$ (b)

11. Conclusion

The dynamic response of von-Kármán plate with damping is always a difficult subject in vibration mechanics. A general finite element method based on fictive force field has been proposed to facilitate the calculation of in-plane slipping, it also enables the revealing of hardening/softening effect. This method provides the possibility of an accelerated estimation of structure's damped response. A rectangular plate with different slipping boundary condition is used for demonstrating the single and multi-mode method. The analyze of participation factors which issue from the notion of non-linear mode shows that single mode method is adequate for symmetric boundary conditions and is sufficient even in cases with non-symmetric boundaries, but the condition of small displacement must be satisfied. For cases where the displacement symmetry in boundary conditions is broken, it's necessary to take into account the participation of other modes, especially under big modal amplitude.

12. Declaration of conflicting interests

The authors declared no potential conflicts of interest with respect to the research, authorship, and/or publication of this article.

13. Acknowledgments

The authors gratefully acknowledge the financial support of Groupe PSA. The work has been achieved within the framework of the "Vibro-Acoustic-Tribology@Lyon" Openlab.

14. References

- [1] C. Ehrlich, A. Schmidt, L. Gaul, Microslip Joint Damping Prediction Using Thin-Layer Elements, in: Conference Proceedings of the Society for Experimental Mechanics Series, Vol. 1, 2014, pp. 239–244. doi:10.1007/978-3-319-04501-6_22.
- [2] L. Gaul, R. Nitsche, The Role of Friction in Mechanical Joints, Applied Mechanics Reviews 54 (2) (2001) 93. doi:10.1115/1.3097294.
- [3] S. Bograd, A. Schmidt, L. Gaul, Joint damping prediction by thin layer elements, Proceedings of IMAC.
- [4] S. W. E. Earles, Theoretical estimation of the frictional energy dissipation in a simple lap joint, Journal of Mechanical Engineering Science 8 (2) (1966) 207–214.
- [5] M. Masuko, Y. Ito, K. Yoshida, Theoretical Analysis for a damping ratio of a jointed cantilever beam, J. Vet. Med. Science 58 (5) (1996) 481–484. doi:10.1248/cpb.37.3229.
- [6] N. Nishiwaki, M. Masuko, Y. Ito, I. Okumura, A study on damping capacity of a jointed cantilever beam, 1st report, Chem. Pharm. Bull. 14 (1966) 369–375. doi:10.1248/cpb.37.3229.
- [7] B. K. Nanda, A. K. Behera, Study on damping in layered and jointed structures with uniform pressure distribution at the interfaces, Journal of Sound and Vibration 226 (4) (1999) 607–624. doi:10.1006/jsvi.1999.2183.
- [8] B. Singh, B. K. Nanda, Identification of damping mechanism in layered and welded structures, International Journal of Mechanical Sciences 63 (1) (2012) 37–47. doi:10.1016/j.ijmecsci.2012.06.005.
- [9] O. Damisa, V. O. S. Olunloyo, C. Osheku, A. Oyediran, Static analysis of slip damping with clamped laminated beams static analysis of slip damping with clamped laminated beams, European Journal of Scientific Research 17(4) (June 2015) (2007) 455–476.
- [10] O. Damisa, V. O. Olunloyo, C. A. Osheku, A. A. Oyediran, Dynamic analysis of slip damping in clamped layered beams with non-uniform pressure distribution at the interface, Journal of Sound and Vibration 309 (3-5) (2008) 349–374. doi:10.1016/j.jsv.2007.03.066.
- [11] H. Xiao, Y. Shao, J. Xu, Investigation into the energy dissipation of a lap joint using the one-dimensional microslip friction model, European Journal of Mechanics, A/Solids 43 (2014) 1–8. doi:10.1016/j.euromechsol.2013.08.003.
- [12] L. Jezequel, Structural damping by slip in joints, Journal of vibration, acoustics, stress and reliability in design 105 (81) (1983) 497–504. doi:10.1115/1.3269134.
- [13] N. Peyret, J.-L. Dion, G. Chevallier, P. Argoul, Micro-Slip Induced Damping in Planar Contact Under Constant and Uniform Normal Stress, International Journal of Applied Mechanics 02 (02) (2010) 281–304. doi:10.1142/S1758825110000597.
- [14] S. Woinowsky-Krieger, The effect of an axial force on the vibration of hinged bars, Journal of Applied Mechanics 17 (1) (1950) 35–36.

- [15] H. U. Akay, Dynamic large deflection analysis of plates using mixed finite elements, *Computers & Structures* 11 (1-2) (1980) 1–11. doi:10.1016/0045-7949(80)90142-X.
- [16] R. M. Kirby, Z. Yosibash, Solution of von-Kármán dynamic non-linear plate equations using a pseudo-spectral method, *Computer Methods in Applied Mechanics and Engineering* 193 (6-8) (2004) 575–599. doi:10.1016/j.cma.2003.10.013.
- [17] I. Bock, J. Jarušek, M. Šilhavý, On the solutions of a dynamic contact problem for a thermoelastic von Kármán plate, *Nonlinear Analysis: Real World Applications* 32 (2016) 111–135. doi:10.1016/j.nonrwa.2016.04.004.
- [18] X. Huang, Optimization of dynamic behavior of assembled structures based on generalized modal synthesis, Theses, Université de Lyon (Nov. 2016).
URL <https://tel.archives-ouvertes.fr/tel-01539041>